

Sub-micrometer yttrium iron garnet LPE films with low ferromagnetic resonance losses

Carsten Dubs,¹ Oleksii Surzhenko,¹ Ralf Linke,¹ Andreas Danilewsky,² Uwe Brückner,³ and Jan Dellith³

¹*INNOVENT e.V., Technologieentwicklung, Prüssingstr. 27B, 07745 Jena, Germany*

²*Kristallographie, Albert-Ludwigs-Universität Freiburg, Hermann-Herder-Str. 5, 79104 Freiburg, Germany*

³*Leibniz-Institut für Photonische Technologien (IPHT), Albert-Einstein-Str. 9, 07745 Jena, Germany*

(Dated: 30 August 2016)

Using liquid phase epitaxy (LPE) technique (111) yttrium iron garnet (YIG) films with thicknesses of ≈ 100 nm and surface roughnesses as low as 0.3 nm have been grown as a basic material for spin-wave propagation experiments in microstructured waveguides. The continuously strained films exhibit nearly perfect crystallinity without significant mosaicity and with effective lattice misfits of $\Delta a^\perp/a_s \approx 10^{-4}$ and below. The film/substrate interface is extremely sharp without broad interdiffusion layer formation. All LPE films exhibit a nearly bulk-like saturation magnetization of (1800 ± 20) Gs and an ‘easy cone’ anisotropy type with extremely small in-plane coercive fields < 0.2 Oe. There is a rather weak in-plane magnetic anisotropy with a pronounced six-fold symmetry observed for saturation field < 1.5 Oe. No significant out-of-plane anisotropy is observed, but a weak dependence of the effective magnetization on the lattice misfit is detected. The narrowest ferromagnetic resonance linewidth is determined to be 1.4 Oe @ 6.5 GHz which is the lowest values reported so far for YIG films of 100 nm thicknesses and below. The Gilbert damping coefficient for investigated LPE films is estimated to be close to 1×10^{-4} .

PACS numbers: 81.15.Lm, 75.50.Gg, 76.50.+g

I. INTRODUCTION

Magnonics is an increasingly growing new branch of spin-wave physics, specifically addressing the use of magnons for information transport and processing^{1–4}. Single crystalline yttrium iron garnet (YIG), which is a ferrimagnetic insulator with the smallest known magnetic relaxation parameter⁵, appears to be a superior candidate for this purpose^{6–8}. As bulk or as thick film material, which is commonly grown by liquid phase epitaxy (LPE)⁹, it has a very low damping coefficient and allows magnons to propagate over distances exceeding several centimeters⁶. However YIG functional layers for practical magnonics should be nanometer-thin with extremely smooth surfaces in order to achieve optimum efficiency in data processing and dramatic reduction in energy consumption of sophisticated spin-wave devices. Therefore, high-quality thin and ultra-thin YIG films were grown using different growth techniques such as LPE, pulsed laser deposition (PLD) and rf-magnetron sputtering to investigate diverse spin-wave effects and to design YIG waveguides as well as nanostructures for spin wave excitation, manipulation and detection in prospective magnonic circuits.

From previous reports about sub-micrometer YIG films with thicknesses between 100 and 20 nm^{10–15} available microwave and magnetic key parameters were taken and summarized in Table I. Thus, ferromagnetic resonance (FMR) data were included which have been extracted from measurements of the absorption curves or absorption derivative curves versus sweeping magnetic in-plane field H at a fixed frequency f or vs. sweep-

ing rf-exciting field h_{rf} with an applied in-plane static magnetic bias field. The reported FMR linewidths ΔH and converted peak to peak linewidths ΔH_{p-p} of the field derivative values ($\Delta H = \sqrt{3} \Delta H_{p-p}$), which will be given during the further paper as full-width at half-maximum ΔH_{FWHM} , varied between 3 Oe and 13 Oe. The Gilbert damping coefficient α were found in the range from 2×10^{-4} to 8×10^{-4} . Only the lowest given α value of 0.9×10^{-4} was obtained for a very short fit range of about 4 GHz without any given data in the low frequency range below 10 GHz¹³ and is therefore not really comparable with the other reported values. From this compilation it is obvious that neither ΔH_{FWHM} nor α is significantly influenced by the YIG film thickness down to 20 nm. The differences are probably resulted from additional ferromagnetic losses due to contributions of homogeneous and/or inhomogeneous broadening by microstructural imperfections or magnetic inhomogeneities.

In this report we present microstructural, magnetic and FMR properties of LPE-grown 100 nm thin YIG and Lanthanum substituted (La:YIG) films with low ferromagnetic resonance losses. Film thicknesses were determined by X-ray reflectometry (XRR) and surface roughness by atomic force microscopy (AFM) measurements. Crystalline perfection and compositional homogeneity were investigated by high-resolution X-ray diffraction (HR-XRD) and X-ray photoelectron spectroscopy (XPS) as well as by secondary ion mass spectroscopy (SIMS). Static and dynamic (microwave) magnetic characterizations were carried out by vibrating sample magnetometry (VSM) and by Vector Network Analysis (VNA), respectively.

TABLE I: Key parameters reported for thin/ultrathin YIG films on (111) GGG substrates

Growth method (Reference)	Thick- ness (nm)	RMS- roughness (nm)	$4\pi M_s^a$ (kGs)	H_c^a (Oe)	ΔH^a FWHM (Oe)	f_0 (GHz)	ΔH_0^a FWHM (Oe)	α $\times 10^{-4}$
LPE ¹⁰	100	-	1.81	-	3.0	7	1.6	2.8
LPE (this study)	83–113	0.3–0.8	1.78–1.82	≤ 0.2	1.4–1.6	6.5	0.5–0.7	1.2–1.7
PLD ^{b 11}	79	0.2	1.72	< 2	3.0	10	1.4	2.2
PLD ¹²	23	-	1.60	< 1	3.5 ^c	9.6	3.5–7 ^c	2–4
Sputtering ¹³	22	0.13	1.78	0.4	12 ^c	16.5	6.4 ^c	0.9
Sputtering ¹⁴	20	0.2	-	0.4	13 ^c	9.7	7 ^c	8
PLD ¹⁵	20	0.2–0.3	2.10	0.2	3.3 ^c	6	2.4 ^c	2.3

^a Measurements at RT with the in-plane external magnetic field H

^b YIG films grown on the (100) GGG substrates

^c Peak-to-peak value ΔH_{p-p} of the derivative of FMR absorption transformed into $\Delta H_{FWHM} = \Delta H_{p-p} \times \sqrt{3}$

II. RESULTS

A. Microstructural properties

Selected microstructural and magnetic properties of liquid phase epitaxial grown YIG (sample A-C) and La:YIG (sample D) films are given in Table II. The consistent magnetic as well as microwave properties obtained for films deposited during different growth runs demonstrate a high reproducibility of the LPE growth technique. Fig. 1a shows XRR plots of films with thicknesses of about 100 nm which are smaller than the previously reported thinnest LPE YIG films^{16–18}. The smallest root-mean-square (RMS) surface roughness of about 0.25 nm obtained for the sample B in Fig. 1b is nearly comparable with epi-polished GGG substrate quality of ≈ 0.15 nm and with the best PLD and sputtered YIG films (see e.g. Table I). Besides, films with slightly rougher surfaces (see Table II) were obtained as a result of additional dendritic aftergrowth and/or due to plateau formation, so called “mesas”, if any solution droplet adheres to the sample surface.

HR-XRD studies of our thin epitaxial LPE films have been found to be difficult because of the nearly superimposed diffraction pattern of YIG film and GGG substrate. Although the angle distances between film and substrate Bragg reflections were above the resolution limit of our HR-XRD equipment, the diffraction intensity of the film reflection was very low and results only in a broadening of the GGG Bragg reflection. Fig. 2a shows a ω -scan (rocking curve) with a Gaussian-like fitted GGG substrate 444 reflection and a second fitted peak at the right shoulder which corresponds to the YIG 444 film reflection. This indicates a tensile stressed YIG film because of the smaller film lattice parameter compared to the commercially available Czochralski-grown GGG substrate ($a_s = 1.2382$ nm). For La:YIG films we observed a perfect pseudo-Voigt fitted substrate peak without any additional shoulder (not shown) which indicates

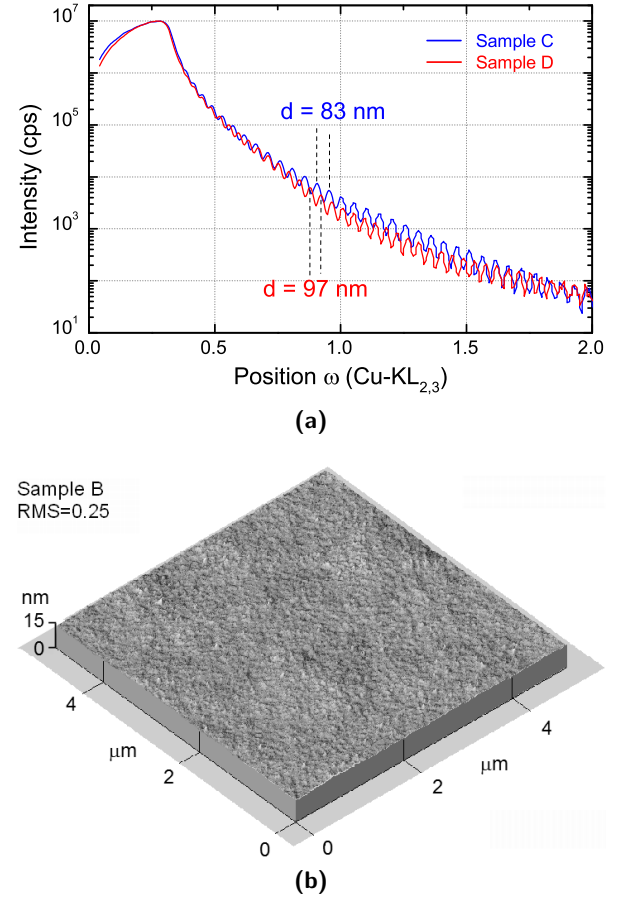


FIG. 1: (a) XRR plots of sub-micrometer-thick YIG LPE films. (b) $5 \times 5 \mu m^2$ AFM surface topography of sample B with RMS roughness of 0.25 nm.

a perfect lattice match between substrate and LPE film. This is in remarkable contrast to YIG films deposited by various gas phase techniques such as PLD and rf-

TABLE II: YIG/La:YIG film properties grown on (111) GGG substrates by LPE technology

Sample	Thick- ness (nm)	RMS- roughness (nm)	Relative lattice misfit $\Delta a^\perp/a_s$ $\times 10^{-4}$	VSM ^a		FMR ^a			
				$4\pi M_s$ (kGs)	H_c (Oe)	$4\pi M_{\text{eff}}$ (kGs)	ΔH_{FWHM}^b (Oe)	ΔH_0 (Oe)	α $\times 10^{-4}$
A	113	0.8	4.7	1.82	0.10	1.637	1.4	0.5	1.4
B	106	0.3	1.8	1.78	0.20	1.658	1.5	0.7	1.2
C	83	0.6	0.3	1.82	0.16	1.672	1.4	0.5	1.6
D ^c	97	0.8	0.0	1.78	0.18	1.712	1.6	0.7	1.7
Accuracy	± 1	± 0.1	± 0.3	± 0.04	± 0.03	± 0.010	± 0.1	± 0.1	± 0.1

^a VSM and FMR measurements at room temperature with applied in-plane magnetic field

^b FMR linewidth value at frequency $f=6.5$ GHz

^c La:YIG LPE film

sputtering^{11–15,19,20} on GGG substrates. For those films the YIG reflection has always been detected at considerably lower Bragg angles compared to the GGG substrate indicating a significant distortion of the cubic YIG garnet cell with significantly enlarged lattice parameters (compressive stress)^{19,21}.

The relative effective misfit $\Delta a^\perp/a_s = (a_s - a_{\text{YIG}}^\perp)/a_s$ obtained from strained film lattice parameter in growth direction a_{YIG}^\perp and the substrate lattice parameter a_s can be used as a measure for epitaxial induced in-plane tension or strain. Due to YIG Poisson's ratio of $\nu_P = 0.29$ pseudomorphously grown, fully strained YIG films with an ideal YIG_{bulk} lattice parameter $a_{\text{YIG}} = 1.2375 \text{ nm}^{22}$ should have a relative effective misfit of $\Delta a^\perp/a_s = +11 \times 10^{-4}$ (tensile stress). In the case of our sub-micrometer YIG films $\Delta a^\perp/a_s$ has been determined to be in the range between zero and $+5 \times 10^{-4}$ (see Table II) compared to PLD-grown YIG films with up to $\Delta a^\perp/a_s = -100 \times 10^{-4}$ (see e.g. Ref.12). Hence, our LPE films are under tension but not to the extent which we expected for nominally pure YIG material without additional lattice expansion by lattice defects or impurities. To find the reason for this, high-resolution reciprocal space map (HR-RSM) and XPS investigations were performed. Fig. 2b shows a HR-RSM plot around the symmetrical 444 Bragg reflection with symmetrical diffracted intensity for the GGG substrate and asymmetric diffracted intensity toward higher scattering angles along Q_z (2θ - ω -Scan) which we attribute to the YIG 444 film reflection. Broadening of the film reflection along Q_z is due to the finite coherence length of the sub-micrometer thin film in growth direction and other broadening mechanisms as for example heterogeneous strain. The extension of the film reflection up to the substrate peak position suggests that the film is continuously strained due to an existing compositional and/or strain gradient. No peak broadening along the Q_x direction (ω -scan) indicates single crystalline perfection parallel to the film plane without significant mosaicity due to tilts of epitaxial regions with respect to one another.

To evaluate the compositional homogeneity along the

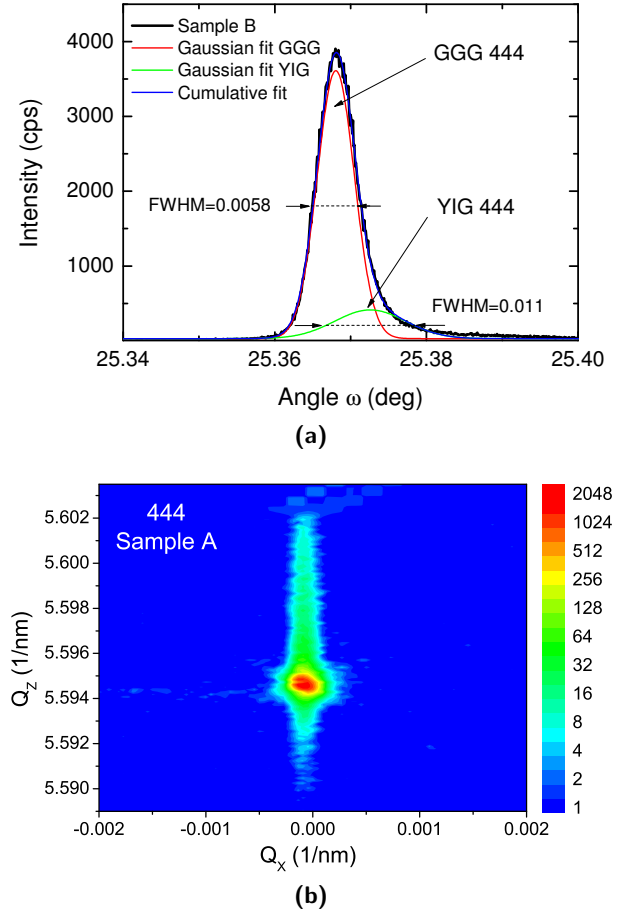


FIG. 2: (a) HR-XRD ω -scan around substrate/film 444 Bragg reflection of sample B. By fitting procedures the YIG film peak has been extracted. (b) HR-RSM scans around substrate/film 444 reciprocal point reveal asymmetric diffracted intensities towards higher Q_z values for sample A.

growth direction of the films and to detect expected impurities (e.g. Pb from solvent) depth profile analy-

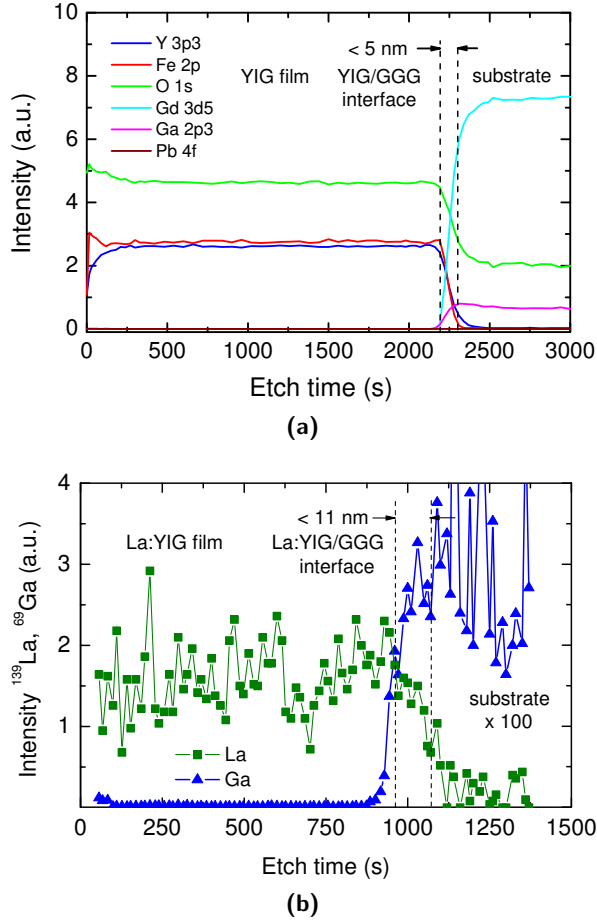


FIG. 3: (a) XPS depth profile of sample B reveals a very narrow interface between film and substrate. The Pb 4f signal could not be detected within the detection limit of about 0.1 at-%. (b) SIMS depth profile analysis detects the ^{139}La signal of the film as well as the ^{69}Ga signal of the substrate (sample D) and their changes at the film/substrate interface.

ses were carried out by XPS. Fig. 3a shows a homogeneous distribution of the YIG matrix elements along the film growth direction and a sharp transition at the film/substrate interface. The obtained width of the transition layer for sample B is below 5 nm. But the obtained depth profile consists of a convolution of the true concentration profile with the depth resolution of the XPS system under the concrete measuring conditions and should be narrower. Therefore, these profiles demonstrate that no broad interdiffusion layer is formed by element intermixing at the interface at an early state of epitaxial growth or by diffusion of substrate ions into the epitaxial layer and vice versa during the subsequent growth process.

Whereas XPS surface analysis of the very first atomic layers (not shown) gives a Pb content of about 0.2 at-%, no Pb signal could be observed during the depth profile

analyses within the detection limit of 0.1 at-%²³. Therefore, it is assumed that the Pb signal corresponds to a surface contamination of condensed PbO vapor from high temperature solution and this contamination is completely removed by the first argon-ion etching step. For YIG films grown in La_2O_3 containing solution no La signal could be detected by XPS that give indicates that the La content must be below 0.5 at-%²⁴. In order to improve the detection capability additional qualitative SIMS measurements were carried out. Due to the resulting sputtering effect and by time-dependent detection of the sputtered sample ions one obtains depth profiles of the film elements as shown for ^{139}La in Fig. 3b. Here, the counts of two separate measurements taken under identical measuring conditions at neighboring sample positions were added up in order to enhance the statistical significance. It is clearly visible that the lanthanum signal decreases at the film/substrate interface whereas substrate signals like ^{69}Ga simultaneously increase.

B. Static magnetic measurements

The vibrating sample magnetometry was used to measure the net magnetic moment m of the YIG/GGG samples at room temperature. As a thickness of GGG substrates ≈ 5000 times exceeded these of the studied YIG films, a proper calculation of the YIG parameters required us (i) to extract the GGG contribution that linearly increased with the external field H and (ii) to prefer the in-plane sample orientation that ensured considerably lower fields H_s for the YIG films to attain the saturation.

Fig. 4a presents a typical dependence of the total magnetic moment m vs the in-plane magnetic field H and illustrates the method allowing us to separate the m' components produced by the YIG film and the GGG substrate. Being subsequently normalized to the film volume, the YIG component loops yield the following material parameters – a saturation magnetization M_s , a coercivity H_c and a saturation field H_s , i.e. the field (averaged over ascending H_\uparrow and descending H_\downarrow branches of hysteresis loops) where the YIG film magnetization approaches $0.9 \times M_s$. In order to estimate the in-plane anisotropy, we have repeated this procedure for the samples rotated around the $\langle 111 \rangle$ axis perpendicular to film surfaces. Fig. 4b demonstrates such results as polar semi-log plots vs the azimuthal angle φ . A saturation magnetization M_s in Fig. 4b seems independent of φ . The obtained $4\pi M_s$ values cluster around 1800 Gs usually reported²⁵ for bulk YIG single crystals. Within an experimental error (mostly defined by the YIG volume uncertainty of $\pm 2\%$), the same is valid for the $4\pi M_s$ values in other LPE films listed in Table II. The obtained coercivity ($H_c \leq 0.2$ Oe) in studied LPE films is among the best values reported for gas phase epitaxial films (see Table I). No distinct influence of the crystallographic orientation on the H_c values is also registered. In contrast, the azimuthal dependence of the saturation field H_s ob-

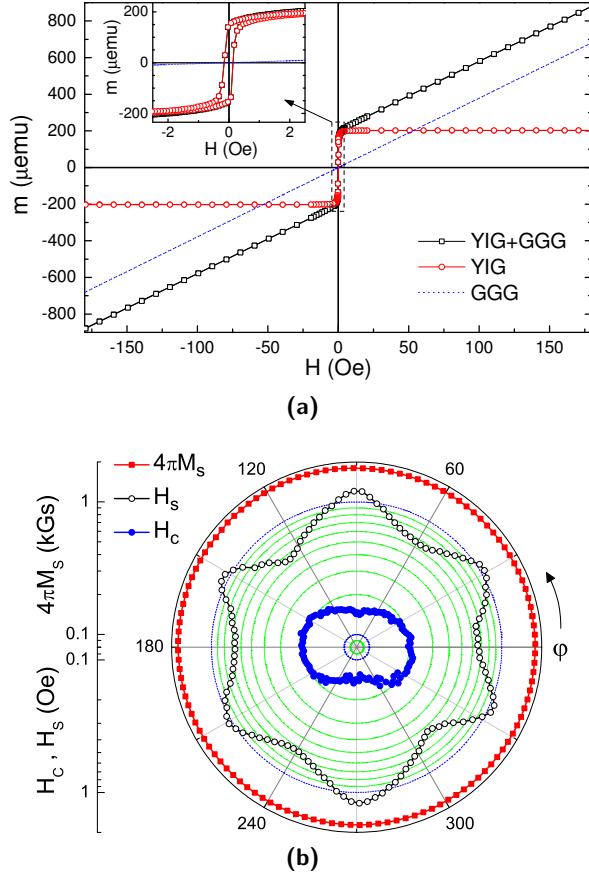


FIG. 4: (a) The net VSM magnetic moment m of the sample D as well as its components induced by the YIG film and the GGG substrate vs the in-plane magnetic field H parallel to the $\langle 110 \rangle$ direction. (b) Azimuthal angle dependencies for the VSM loop parameters of sample D, i.e. a saturation magnetization M_s , a saturation field H_s and a coercivity H_c . The H_s six-fold symmetry with the minima along the $\langle 112 \rangle$ ‘easy axes’ and the maxima along the $\langle 110 \rangle$ ‘hard axes’ indicates the cubic magnetocrystalline anisotropy.

viously reveals the six-fold symmetry which matches the crystallographic symmetry of YIGs. The H_s maxima coincide with the in-plane $\langle 110 \rangle$ projections of the hard magnetization axes, whereas the H_s minima correspond to the $\langle 112 \rangle$ crystallographic directions. The $\langle 112 \rangle$ ‘easy axes’ orientation suggests an ‘easy cone’ anisotropy after Ubizskii²⁶. He has also demonstrated²⁷ that relatively small in-plane magnetic fields lead to single-domain YIG films, although a deviation of magnetization vector from the film plane still remains due to finite values of the cubic anisotropy constants.

In conclusion, as the demagnetizing factor at the out-of-plane YIG film orientation is 1, the out-of-plane saturation field has to be close to the in-plane $4\pi M_s$ values. This fact is qualitatively confirmed by our out-of-plane measurements. Unfortunately, the GGG component of

the total VSM signal at fields $H_{\perp} \approx 1.8$ kOe is much larger than magnetic moments of YIG films with a thickness of ≈ 100 nm (see, for instance, Fig. 4a) and, hence, a reasonable accuracy of $\pm 0.5\%$ at the GGG signal elimination inevitably results in too large errors for the YIG parameters. One may conclude that the out-of-plane configuration may provide reliable results when the ratio of YIG to GGG thickness exceeds, at least, 10^{-3} .

C. FMR absorption

FMR absorption spectra for each of studied YIG films were recorded at several values ($H \leq 5$ kOe) of the in-plane magnetic field. The inset in Fig. 5 shows such a spectrum at $H = 1.6$ kOe that looks like the Lorentz function with a linewidth $\Delta f_{\text{FWHM}} \approx 4$ MHz centered near the FMR frequency $f \approx 6.5$ GHz. Since the FMR linewidth is mostly expressed in units of magnetic field, we, at first, used the centers f of measured spectra and the corresponding in-plane fields H to estimate the gyromagnetic ratio γ and the effective magnetization M_{eff} in the Kittel formula²⁸

$$f = \gamma \sqrt{H(H + 4\pi M_{\text{eff}})}. \quad (1)$$

Then, the best fitting pair of γ and M_{eff} allowed us (i) to convert every frequency spectrum into the magnetic field scale, (ii) to fit rescaled spectra with the Lorentz function and (iii) to evaluate, thereby, the corresponding linewidth ΔH_{FWHM} . The selected results of the described procedure – namely, $4\pi M_{\text{eff}}$ and ΔH_{FWHM} at the reference frequency $f = 6.5$ GHz – are listed in Table II, while the whole summary of the obtained ΔH_{FWHM} values is

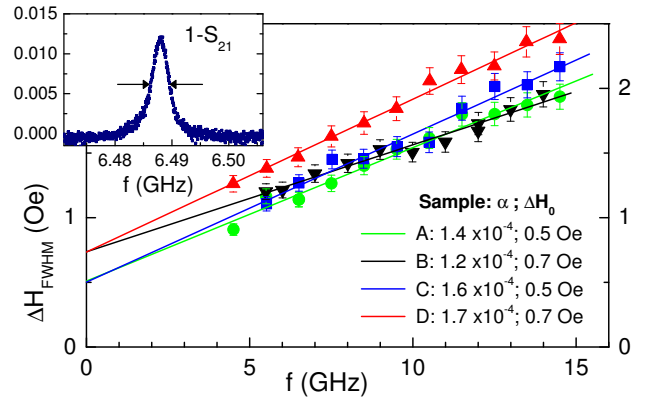


FIG. 5: Frequency dependence of FMR absorption linewidth ΔH_{FWHM} for YIG LPE films A–D at various values of the in-plane magnetic field ($H \leq 5$ kOe). Straight lines are linear fits that the Gilbert damping factors α are obtained from. Inset shows an example of FMR absorption spectrum measured for the sample A at $H = 1.6$ kOe.

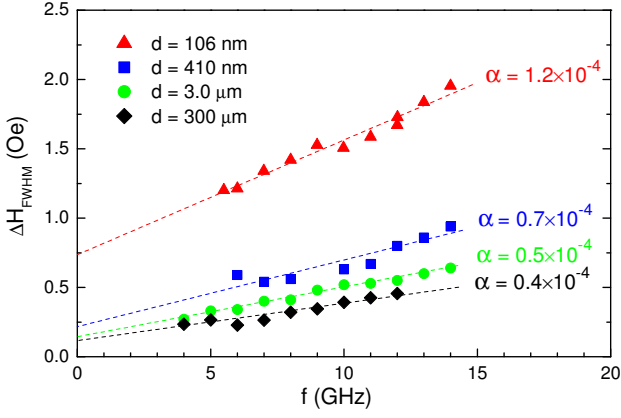


FIG. 6: Frequency dependencies of the FMR linewidth ΔH_{FWHM} for YIG LPE films of various thickness d and the YIG sphere with diameter $d = 300 \mu\text{m}$. The Gilbert damping factors α are calculated from slopes of the best linear fits according to Eq. (2).

presented in Fig. 5 vs the FMR frequency. The plots in Fig. 5 are known^{10–14} to provide data about the Gilbert damping coefficient α and the inhomogeneous contribution ΔH_0 to the FMR linewidth that are mutually related by

$$\Delta H_{\text{FWHM}} = \Delta H_0 + \frac{2\alpha f}{\gamma} \quad (2)$$

As the FMR performance of thin YIG films strongly depends on the working frequency of future magnonic applications, we have included various quality parameters in Table II, *viz.* i) the Gilbert damping coefficient α which is mostly responsible for the FMR losses at high magnetic fields ($H \gg 4\pi M_{\text{eff}}$), ii) the inhomogeneous contribution ΔH_0 that dominates at small fields ($H \ll 4\pi M_{\text{eff}}$) as well as iii) the FMR linewidth at the reference frequency $f = 6.5 \text{ GHz}$ which approximately corresponds to the case $H \approx 4\pi M_{\text{eff}}$. The latter is estimated down to $\Delta H_{\text{FWHM}} = 1.4 \text{ Oe}$ that is to our knowledge the narrowest value reported so far for YIG films with a thickness of about 100 nm and smaller. The Gilbert damping coefficients are estimated to be close to $\alpha \approx 1 \times 10^{-4}$ which is comparable to the best values reported so far (compare with Table I). The zero frequency term ΔH_0 is found almost the same for all YIG films including the La substituted one. The obtained value $\Delta H_0 \approx 0.5 - 0.7 \text{ Oe}$ appears as well appreciably lower than that for gas phase epitaxial films (see Table I).

In summary, optimized LPE growth and post-processing conditions improve FMR linewidths and Gilbert damping coefficients (compare this study and Ref.29 with Ref.10). However, the improved values are still far from these in bulk YIGs and relatively thick YIG films (see Fig. 6) due to the decreasing volume to interface ratio in sub-micrometer films. For example, imperfections at the film interface of thin films should have a

stronger influence on the magnetic losses in contrast to the dominating volume properties of perfect thick films. It requires us to undertake further attempts to minimize the FMR performance deterioration with a decrease of the YIG film thickness. These attempts will be focused on avoiding the most probable sources of FMR losses such as contributions due to homogeneous broadening (interface roughness, homogeneously distributed defects and impurities) and inhomogeneous broadening (geometric and magnetic mosaicity, single surface defects) and, thus, on approaching the “target” parameters of $\Delta H_{\text{FWHM}} = 0.3 \text{ Oe}$ at 6.5 GHz and $\alpha = 0.4 \times 10^{-4}$ reported by Röschmann and Tolkdorf³⁰ for bulk discs made of single YIG crystals.

III. OUTLOOK AND CONCLUSIONS

Besides the efforts to avoid growth defects as well as interface roughness and to reduce impurity incorporation during the LPE deposition process further high-resolution investigations are necessary to gain more insight into the YIG microstructure and to identify the properties which play an essential role for its FMR performance. Therefore, in future studies we will carry out HR-RSM scans with asymmetrical reflections to determine in-plane and axial strain, respectively, the Time-of-Flight (ToF) SIMS analysis technique using element standards to precisely quantify the La substitution concentration as well as to detect impurity elements from the high-temperature solutions in our sub-micrometer LPE films. Furthermore, angular dependent measurements of the resonance field and of the FMR linewidth will be intended to determine the influence of uniaxial magnetic anisotropies on the ferromagnetic resonance losses.

In conclusion, liquid phase epitaxy has the potential to provide sub-micrometer YIG films with outstanding crystalline and magnetic properties to meet the requirements for future magnon spintronics with ultra-low effective losses if a drastic miniaturization down to the nanometer scale is possible. First sub-100 nm lateral sized structures have presently been prepared³¹ which could be the next step to LPE-based microscaled spintronic circuits. The development of YIG LPE films with thicknesses below 100 nm is now in progress and remains a big challenge for the classical thick-film LPE technique.

IV. METHODS

A. Sample fabrication

YIG films were grown from $\text{PbO-B}_2\text{O}_3$ based high-temperature solutions resistively-heated in a platinum crucible at about 900°C using standard dipping LPE technique. During different growth runs nominally pure YIG films were grown on one-inch (111) gadolinium gallium garnet (GGG) substrates to check the reproducibil-

ity of the sub-micrometer liquid phase epitaxial growth. For La substituted films La_2O_3 was added to the already used high-temperature solution. To remove solution remnants from the sample surfaces the holder had to be stored in a hot acidic solution after room temperature cooling. Afterwards the reverse side layer was removed by mechanical polishing from the double-side grown samples. Chips of different sizes were prepared by a diamond wire saw and sample surfaces were cleaned using ethanol, distilled water and acetone. The LPE film thickness was determined by X-ray reflectometry using a PANalytical/X-Pert Pro system.

B. Microstructural properties

The root-mean-square surface roughness was determined by AFM measurements for each sample at three different regions over $25\text{ }\mu\text{m}^2$ ranges using a Park Scientific Instruments, M5. HR-XRD studies were performed by a five-crystal diffraction spectrometer of Seifert (3003 PTS HR) equipped with a four-fold Ge 440 asymmetric monochromator using CuK_α radiation. The resolution limit was 1×10^{-4} deg. GGG substrate lattice parameters were obtained by the Bond method. Depth profile analyses were carried out by an Axis Ultra^{DLD} XPS system (Kratos Analytical Ltd.) using a mono-atomic argon-ion etching technique. Qualitative SIMS (Hiden Analytical) measurements were carried out. Here, a film area of $500 \times 500\text{ }\mu\text{m}^2$ is irradiated by 5 keV oxygen ions.

C. Magnetic properties

The vibrating sample magnetometer (MicroSense LLC, EZ-9) was used to register the in-plane hysteresis loops of the YIG/GGG samples at room temperature. The external magnetic field H was controlled with an error of ≤ 0.01 Oe. To estimate the magnetization of the YIG films we removed a contribution of the GGG substrates from the total VSM signal. To monitor the in-plane anisotropy as a function of the crystallographic orientation, the hysteresis loops at the azimuthal angles $0^\circ \leq \varphi \leq 360^\circ$ were measured with an angular step of 3° . The FMR absorption spectra were registered with a vector network analyzer (Rohde & Schwarz GmbH, ZVA 67) attached to a broadband stripline. The sample was disposed face-down over a stripline and the transmission signals (S_{21} & S_{12}) were recorded. During the measurements, a frequency of microwave signals with the input power of -10 dBm (0.1 mW) was swept across the resonance frequency, while the in-plane magnetic field H was constant and measured with an accuracy of 1 Oe. Each recorded spectrum was fitted by the Lorentz function and allowed us to define the resonance frequency and the FMR linewidth ΔH_{FWHM} corresponding to the applied field H .

- ¹V. V. Kruglyak and R. J. Hicken, “Magnonics: Experiment to prove the concept,” *J. Magn. Magn. Mater.* **306**, 191–194 (2006), cond-mat/0511290.
- ²S. Neusser, B. Botters, and D. Grundler, “Localization, confinement, and field-controlled propagation of spin waves in $\text{Ni}_{80}\text{Fe}_{20}$ antidot lattices,” *Phys. Rev. B* **78**, 054406 (2008).
- ³V. V. Kruglyak, S. O. Demokritov, and D. Grundler, “Magnonics,” *J. Phys. D: Appl. Phys.* **43**, 264001 (2010).
- ⁴R. L. Stamps, S. Breitkreutz, J. Åkerman, A. V. Chumak, Y. Otani, G. E. W. Bauer, J.-U. Thiele, M. Bowen, S. A. Majetich, M. Kläui, I. Lucian Prejbeanu, B. Dieny, N. M. Dempsey, and B. Hillebrands, “The 2014 Magnetism Roadmap,” *J. Phys. D: Appl. Phys.* **47**, 333001 (2014), arXiv:1410.6404 [cond-mat.mtrl-sci].
- ⁵R. C. LeCraw, E. G. Spencer, and C. S. Porter, “Ferromagnetic Resonance Line Width in Yttrium Iron Garnet Single Crystals,” *Phys. Rev.* **110**, 1311–1313 (1958).
- ⁶A. A. Serga, A. V. Chumak, and B. Hillebrands, “YIG magnonics,” *J. Phys. D: Appl. Phys.* **43**, 264002 (2010).
- ⁷A. V. Chumak, A. A. Serga, and B. Hillebrands, “Magnon transistor for all-magnon data processing,” *Nat. Commun.* **5**, 4700 (2014).
- ⁸A. V. Chumak, V. I. Vasyuchka, A. A. Serga, and B. Hillebrands, “Magnon spintronics,” *Nat. Phys.* **11**, 453–461 (2015).
- ⁹E. A. Giess, J. D. Kuptsis, and E. A. D. White, “Liquid phase epitaxial growth of magnetic garnet films by isothermal dipping in a horizontal plane with axial rotation,” *J. Cryst. Growth* **16**, 36–42 (1972).
- ¹⁰P. Pirro, T. Brächer, A. V. Chumak, B. Lägél, C. Dubs, O. Surzhenko, P. Gönert, B. Leven, and B. Hillebrands, “Spin-wave excitation and propagation in microstructured waveguides of yttrium iron garnet/Pt bilayers,” *Appl. Phys. Lett.* **104**, 012402 (2014), arXiv:1311.6305 [cond-mat.mes-hall].
- ¹¹M. C. Onbasli, A. Kehlberger, D. H. Kim, G. Jakob, M. Kläui, A. V. Chumak, B. Hillebrands, and C. A. Ross, “Pulsed laser deposition of epitaxial yttrium iron garnet films with low Gilbert damping and bulk-like magnetization,” *APL Mater.* **2**, 106102 (2014).
- ¹²B. M. Howe, S. Emori, H.-M. Jeon, T. Oxhol, J. G. Jones, K. Mahalingam, Y. Zhuang, N. X. Sun, and G. J. Brown, “Pseudomorphic yttrium iron garnet thin films with low damping and inhomogeneous linewidth broadening,” *IEEE Magn. Lett.* **8**, 3500504 (2015).
- ¹³H. Chang, P. Li, W. Zhang, T. Liu, A. Hoffmann, L. Deng, and M. Wu, “Nanometer-thick yttrium iron garnet films with extremely low damping,” *IEEE Magn. Lett.* **5**, 6700104 (2014).
- ¹⁴H. Wang, *Understanding of Pure Spin Transport in a Broad Range of $\text{Y}_3\text{Fe}_5\text{O}_{12}$ -based Heterostructures*, Ph.D. thesis, The Ohio State University (2015).
- ¹⁵O. d’Allivy Kelly, A. Anane, R. Bernard, J. Ben Youssef, C. Hahn, A. H. Molpeceres, C. Carrétéro, E. Jacquet, C. Deranlot, P. Bortolotti, R. Lebourgeois, J.-C. Mage, G. de Loubens, O. Klein, V. Cros, and A. Fert, “Inverse spin Hall effect in nanometer-thick yttrium iron garnet/Pt system,” *Appl. Phys. Lett.* **103**, 082408 (2013), arXiv:1308.0192 [cond-mat.mtrl-sci].
- ¹⁶V. Castel, N. Vlietstra, B. J. van Wees, and J. B. Youssef, “Frequency and power dependence of spin-current emission by spin pumping in a thin-film YIG/Pt system,” *Phys. Rev. B* **86**, 134419 (2012), arXiv:1206.6671 [cond-mat.mtrl-sci].
- ¹⁷C. Hahn, G. de Loubens, O. Klein, M. Viret, V. V. Naletov, and J. Ben Youssef, “Comparative measurements of inverse spin Hall effects and magnetoresistance in YIG/Pt and YIG/Ta,” *Phys. Rev. B* **87**, 174417 (2013), arXiv:1302.4416 [cond-mat.mes-hall].
- ¹⁸L. J. Cornelissen, J. Liu, R. A. Duine, J. B. Youssef, and B. J. van Wees, “Long-distance transport of magnon spin information in a magnetic insulator at room temperature,” *Nat. Phys.* **11**, 1022–1026 (2015), arXiv:1505.06325 [cond-mat.mes-hall].
- ¹⁹S. A. Manuilov, R. Fors, S. I. Khartsev, and A. M. Grishin, “Sub-micron $\text{Y}_3\text{Fe}_5\text{O}_{12}$ Film Magnetostatic Wave Band Pass Filters,” *J. Appl. Phys.* **105**, 033917–033917 (2009).

- ²⁰Y. Sun, Y.-Y. Song, H. Chang, M. Kabatek, M. Jantz, W. Schneider, M. Wu, H. Schultheiss, and A. Hoffmann, “Growth and ferromagnetic resonance properties of nanometer-thick yttrium iron garnet films,” *Appl. Phys. Lett.* **101**, 152405 (2012).
- ²¹S. A. Manuilov, S. I. Khartsev, and A. M. Grishin, “Pulsed laser deposited $\text{Y}_3\text{Fe}_5\text{O}_{12}$ films: Nature of magnetic anisotropy I,” *J. Appl. Phys.* **106**, 123917–123917 (2009).
- ²²R. Hergt, H. Pfeiffer, P. Görnert, M. Wendt, B. Keszei, and J. Vandlik, “Kinetic Segregation of Lead Impurities in Garnet LPE Films,” *Phys. Stat. Sol. (a)* **104**, 769–776 (1987).
- ²³0.1 at-% Pb corresponds to $x_{\text{Pb}} \approx 0.02$ formula units in stoichiometric $\text{Y}_{3-x}\text{Pb}_x\text{Fe}_5\text{O}_{12}$.
- ²⁴0.5 at-% La corresponds to $y_{\text{La}} \approx 0.1$ formula units in stoichiometric $\text{Y}_{3-y}\text{La}_y\text{Fe}_5\text{O}_{12}$.
- ²⁵G. Winkler, “Magnetic garnets,” in *Vieweg tracts in pure and applied physics; Volume 5* (Friedrich Vieweg & Sohn Verlag, Braunschweig, Wiesbaden, 1981) Chap. 2, pp. 75–79.
- ²⁶S. B. Ubizskii, “Orientational states of magnetization in epitaxial (111)-oriented iron garnet films,” *J. Magn. Magn. Mater.* **195**, 575–582 (1999).
- ²⁷S. B. Ubizskii, “Magnetization reversal modelling for (111)-oriented epitaxial films of iron garnets with mixed anisotropy,” *J. Magn. Magn. Mater.* **219**, 127–141 (2000).
- ²⁸C. Kittel, “On the Theory of Ferromagnetic Resonance Absorption,” *Phys. Rev.* **73**, 155–161 (1948).
- ²⁹V. Lauer, D. A. Bozhko, T. Brächer, P. Pirro, V. I. Vasyuchka, A. A. Serga, M. B. Jungfleisch, M. Agrawal, Y. V. Kobljanskyj, G. A. Melkov, C. Dubs, B. Hillebrands, and A. V. Chumak, “Spin-transfer torque based damping control of parametrically excited spin waves in a magnetic insulator,” *Appl. Phys. Lett.* **108**, 012402 (2016), arXiv:1508.07517 [cond-mat.mes-hall].
- ³⁰P. Röschmann and W. Tolksdorf, “Epitaxial growth and annealing control of FMR properties of thick homogeneous Ga substituted yttrium iron garnet films,” *Mat. Res. Bull.* **18**, 449–459 (1983).

- ³¹T. Löber, A. V. Chumak, and B. Hillebrands, Unpublished results.

V. ACKNOWLEDGEMENTS

We acknowledge the partial financial support by Deutsche Forschungsgemeinschaft (DU 1427/2-1). We thank M. Frigge for EPMA analysis, Ch. Schmidt for XRR measurements and R. Meyer and B. Wenzel for technical support.

VI. AUTHOR CONTRIBUTIONS STATEMENT

C.D. conceived the experiments, prepared all samples and analyzed the data. O.S. performed VSM and FMR measurements and analyzed the data. R.L. performed the XPS experiments. J.D. and U.B. performed the SIMS experiments. A.D. conducted the XRD experiments and analyzed the data. C.D. and O.S. wrote the manuscript. All authors contributed to scientific discussions and the manuscript review.

VII. ADDITIONAL INFORMATION

A. Competing financial interests

The authors declare no competing financial interests.